Kinetic Structure of the Electron Diffusion Region in Antiparallel Magnetic Reconnection

J. Ng, J. Egedal, A. Le, W. Daughton, and L.-J. Chen

Phys. Rev. Lett. **106**, 065002 — Published 10 February 2011

DOI: 10.1103/PhysRevLett.106.065002

Kinetic structure of the electron diffusion region in anti-parallel magnetic reconnection

J. Ng,[1] J. Egedal[a],[1] A. Le,[1] W. Daughton,[2] and L.-J. Chen[3]

[1] *Department of Physics, and Plasma Science and Fusion Center, Massachusetts Institute of Technology, Cambridge, Massachusetts 02139, USA*

[a] *jegedal@psfc.mit.edu*

[2] *Los Alamos National Laboratory, Los Alamos, New Mexico 87545, USA*

[3] *Space Science Center and Physics Department, University of New Hampshire, Durham, NH 03824*

Strong electron pressure anisotropy has been observed upstream of electron diffusion regions during reconnection in the Earth's magnetotail and kinetic simulations. For collisionless anti-parallel reconnection, we find that the anisotropy drives the electron current in the electron diffusion region, and that this current is insensitive to the reconnection electric field. Reconstruction of the electron distribution function within this region at enhanced resolutions reveals its highly structured nature and the mechanism by which the pressure anisotropy sets the structure of the region.

Magnetic reconnection involves a change in topology of the field lines in a plasma, and is thought to play a vital role in a number of plasma processes, including solar flares, sawtooth crashes in tokamaks [1], magnetic substorms in the Earth's magnetosphere and coronal mass ejections. One area of particular interest is the electron diffusion region, where the electron motion decouples from the magnetic field lines, which is necessary for reconnection to occur.

The structure of the electron diffusion region has been studied intensely [2]. In particular, for anti-parallel reconnection, kinetic simulations show that the diffusion region is characterized by a narrow extended layer containing electron jets. Here we show how the jets in the layer are driven by electron pressure anisotropy, $p_\parallel \gg p_\perp$, immediately upstream of the layer rendering the total current in the layer insensitive to the reconnection electric field $E_{\rm rec}$. This mechanism (not included in standard fluid models) is likely to be effective in the Earth's magnetotail, where strong electron pressure anisotropy has been observed by spacecraft upstream of electron diffusion regions [3–5].

We start out by giving a numerical proof that the current in the layer is insensitive to $E_{\rm rec}$. Next we solve Liouville's theorem ($df/dt = 0$) in the field geometry of a kinetic simulation using an analytic form of the anisotropic f as the upstream boundary condition. We thereby reconstruct the full electron distribution inside the layer at a resolution that reveals its highly structured form for the first time. The analysis uncovers the mechanism by which the electron jets are generated by the upstream anisotropy, driving the current in the layer. Our results are thus relevant to NASA's upcoming MMS mission, designed to study the electron scale structure of reconnection regions in the Earth's magnetotail.

For the numerical test, which shows that the net current in the layer is insensitive to the force exerted by $E_{\rm rec}$, we use the fully kinetic particle-in-cell (PIC) simulation described in Ref. [6]. It is translationally symmetric in the y-direction and has a total domain of 2560×2560 cells $= 400d_e \times 400d_e$, where $d_e = c/\omega_{pe}$ is the electron inertial skin depth. The initial state is a Harris sheet characterized by the following parameters: $m_i/m_e = 400$, $T_i/T_e = 5$, $\omega_{pe}/\omega_{ce} = 2$, background density $= 0.3n_0$ and $v_{the}/c = 0.2$. The code tracks roughly 2×10^9 particles and uses open boundary conditions for the particles and fields. Magnetic reconnection develops from a small initial perturbation. We define our coordinate system with the x-axis along the outflow direction, z-axis along the inflow and y-axis into the page. Hence, $E_{\rm rec}$ here equals E_y evaluated at the x-line.

The kinetic simulation is first run in its usual mode up to the time $t\Omega_{\rm ci} = 70$ where the reconnection layer is fully developed. After this time, we modify the simulation scheme as follows: an external force in the y-direction is added on the electrons in a small box around the x-line of dimension $40d_e \times 3d_e$, as shown in Fig. 1(a). The magnitude of this force is equal to the local value of eE_y. In the first simulation the sign of the external force is such that it cancels E_y component of the Lorentz force, while in the second the sign is reversed such that it doubles the force on the electrons from E_y. All other aspects of the simulation scheme remain the same and Maxwell's equations are at all times solved self consistently.

With the force of E_y deactivated, a widening of the electron layer by $\sim 0.5d_e$ is observed and the mean current density at the x-line drops by 26%. Meanwhile, doubling the force of E_y narrows the current layer by $\sim 0.5d_e$ and leads to an increase in the mean current density by 11%. We find that while the current profile J_y varies with the electric field, illustrated in Figs. 1(b) and (c), changes in thickness of the layer ensure that the total out-of-plane current through it remains constant. This is documented further in Figs. 1(d) and (e), where we show the integral of the current density, which (neglecting ion currents) is equivalent to B_x, with the integration constant chosen so that it is equal to zero at $z = 200d_e$. On exiting the layer ($\pm 4d_e$), the integrated current is the same in the simulations with and without the modifications to E_y. This is consistent with the results described in Ref. [7], which showed that momentum balance of the electron layer requires that just upstream of the layer the plasma

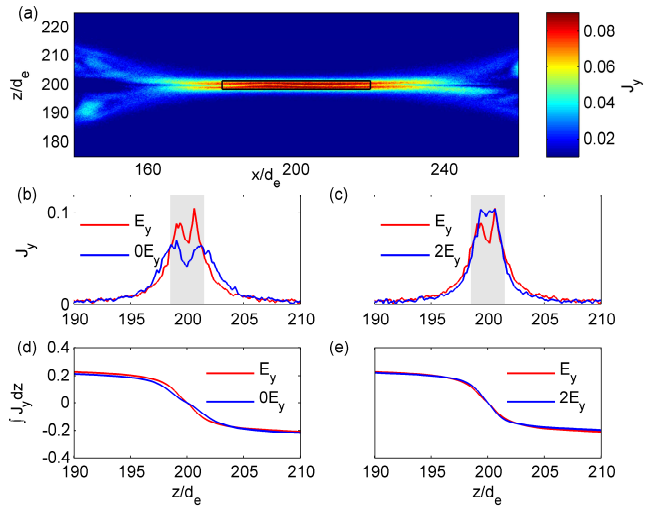

FIG. 1. (color) (a) Out of plane current density J_y in original simulation. The box shows the region where the effect of E_y is modified. Profile of current density at selected times before and during period with (b) no E_y and (c) doubled E_y. Electric field is modified within the shaded region. Integration of J_y across the layer for (d) no E_y and (e) doubled E_y normalized to zero at $z = 200d_e$. Red lines show values from original simulation, blue lines show values with modified E_y. Note that once the interval is extended far enough, the total current is approximately equal to the original current.

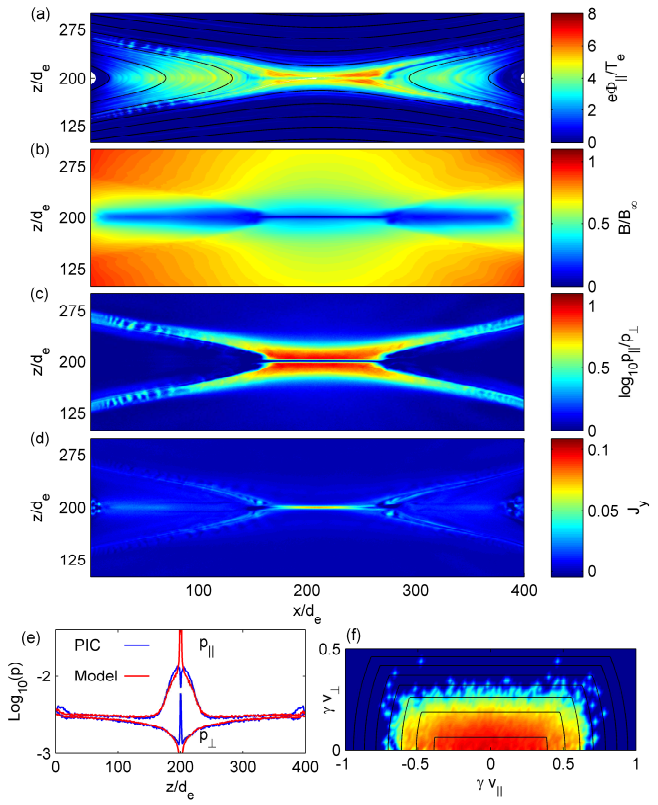

FIG. 2. (color) Time slice from an open-boundary PIC simulation of anti-parallel reconnection. (a) Acceleration potential $e\Phi_\parallel/T_e$. (b) Magnetic field strength B. (c) Pressure ratio $\log_{10}(p_\parallel/p_\perp)$. (d) Out of plane current density J_y. (e) Comparison of $p_\parallel$ and $p_\perp$ from PIC and equations of state for a cut across the x-line. (f) Contours of f with $e\Phi_\parallel/T_e = 4.6$, $B/B_\infty = 0.3$ superimposed over particle data from the inflow of the PIC simulation.

is marginally stable with respect to an electron firehose instability, $B^2 = p_\parallel - p_\perp$. This sets the amplitude of the integrated current independent of $E_{\rm rec}$.

We now proceed to study the internal kinetic properties of the layer and how it is driven by the pressure anisotropy upstream of the layer. In this simulation, with with background density $= 0.23n_0$ and $v_{the}/c = 0.17$, the x-line is at $x = 206.25d_e$ for the time slice considered. In Fig. 2 we show $\Phi_\parallel$, B, $\log_{10}(p_\parallel/p_\perp)$ and J_y. Here the acceleration potential $e\Phi_\parallel(\mathbf{x}) = e\int_{\mathbf{x}}^{\infty}\mathbf{E}\cdot d\mathbf{l}$ (with the integration carried out along the magnetic field lines) is a pseudo potential characterizing the minimal energy required for an electron to escape the region in a straight shot along a field line. It develops to regulate the electron density and maintain quasi neutrality while being the source of the pressure anisotropy [8, 9]. Close to the layer, $e\Phi_\parallel/T_e$ reaches a maximum value of ~ 7 while the ratio $p_\parallel/p_\perp$ reaches ~ 9.

To study the structure of the electron distribution function in the inner layer we make use of a recently derived analytical approximation for the electron distribution upstream of the layer [9]

$$f(\mathbf{x},\mathbf{v}) = \begin{cases} f_\infty\left(\mathcal{E} - e\Phi_\parallel\right), & \text{passing} \\ f_\infty\left(\mu B_\infty\right), & \text{trapped} \end{cases} \qquad (1)$$

where f_∞, the distribution in the ambient plasma, is assumed isotropic, and the trapped passing boundary is described by $\mathcal{E} - e\Phi_\parallel - \mu B_\infty = 0$. The use of this form of the inflow distribution is further justified in Ref. [7]. We also note the good agreement between the equations of state of Ref. [8] (derived from Eq. 1) and the data taken from the PIC simulation up to the point where the magnetic moment breaks down as an adiabatic invariant (Fig. 2(e)). The form of Eq. 1 evaluated at a point in the inflow region is illustrated in Fig. 2(f), and shows good agreement with the simulation particle data.

We can reconstruct the internal distribution $f(\mathbf{x},\mathbf{v})$ at a higher resolution than is available from the particle data from the run by using the fields of the simulation to calculate orbits from a given starting location. By applying initial velocities on an arbitrarily fine grid and following the orbits backwards in time until they reach the region in which Eq. 1 is valid, f can be determined through the use of Liouville's theorem ($df/dt = 0$ along particle trajectories). The reconstructed value, $f(\mathbf{x},\mathbf{v})$, for each point on the grid is obtained directly from Eq. 1 using the values of $\mathcal{E}$, μ and $\Phi_\parallel$ determined at the selected point in the inflow region. Examples of such or-

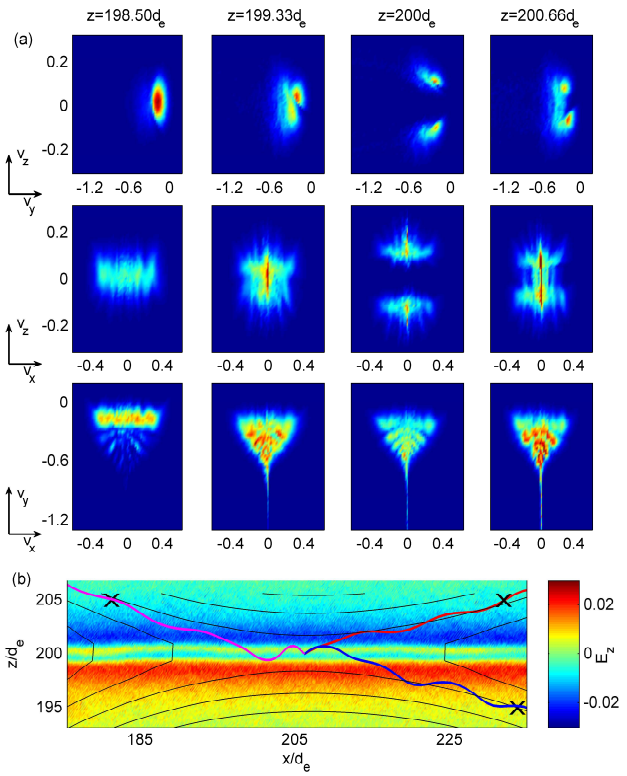

FIG. 3. (color) Plots of distribution function along a cut at $x = 206.25d_e$ and corresponding moments. Velocity units are in terms of c. (a) Distribution function averaged over γv_x, γv_y and γv_z where γ is the Lorentz factor. (b) Electron orbits from x-line with 0, 1 and 2 reflections. Color plot is in-plane electric field E_z, with contours of in-plane projection of magnetic field lines.

bits are depicted in Fig. 3(e) in which the ×'s mark the points at which we evaluate the source distribution function at $5d_e$ upstream of the layer where agreement between Eq. 1 and PIC simulation is good. The large inward pointing E_z shown regulates the entry of electrons into the layer, controlling the density within it (thereby maintaining quasi neutrality).

The resulting distribution from a cut across the layer close to the x-line is shown in Fig. 3(a) where the colored plots show the averaged values over v_x, v_y and v_z respectively. Within the layer, the distribution is highly structured, and we observe a phase space hole in v_z [10], splitting the distribution into two somewhat triangular portions which extend to large values of v_y. Also observed are a number of striations, most noticeable in the v_x-v_y plane. Moving outside the layer, the separation in v_z and extension in v_y decrease, eventually becoming the elongated distribution characteristic of the inflow region.

A more detailed 3-dimensional view of the reconstructed distribution function at locations around the x-line, is shown in Figs. 4(a)-(e). As mentioned earlier, the two main portions of the distribution ($v_z < 0$ and $v_z > 0$) are further divided into numerous striations. Tracing of orbits reveals that each striation is characterized by the number of times the electrons are reflected in the z-direction within the layer before reaching the point of interest, with larger $|v_y|$ corresponding to a larger number of reflections. Such trajectories with 0, 1 and 2 reflections are shown in Fig. 3(e).

To explain the form of the individual striations it is important to note that just upstream of the layer $f(v_\parallel, v_\perp)$ is only large if $\frac{1}{2}mv_\perp^2 \leq T_eB/B_\infty$ and $\frac{1}{2}mv_\parallel^2 \leq e\Phi_\parallel$ where $T_eB/B_\infty \ll e\Phi_\parallel$. We can thus obtain the center of the various striations by injecting electrons parallel to the outside magnetic field ($v_\perp = 0$), with $\frac{1}{2}mv_\parallel^2 \leq e\Phi_\parallel$. As the tip of each striation consists of the highest energy electrons the length of the striations is approximately determined by the acceleration potential $\Phi_\parallel$.

The different parts of the distribution correspond to electrons originating from the four quadrants in the x-z plane. By considering their trajectories, it is clear that those with positive v_x originated from the left of the x-line, and those with negative v_x from the right. The entry z position is determined by the number of reflections and the sign of v_z. For example, the trajectory with two reflections in Fig. 3(e) contributes to the third striation in the bottom-right of the distribution. The entry angle $\angle(v_y, v_x)$ of the parallel streaming electrons is similar to $\angle(B_y, B_x)$ at the entry position. This entry angle and the v_xB_z magnetic forces, which help turn parts of the entry v_x into the y-direction, control the angle between the striations of f in the v_x-v_y plane and varies discrete with the number of reflections. From here, it can be seen how the inflow anisotropy drives the current, as the large parallel steaming velocity of the electrons upstream of the layer gets turned into the y-direction by the entry angle and by the magnetic forces. Finally, the narrow "tip" of the distribution with high number of reflections is due to the longer time this limited class of electrons are accelerated by E_y.

For comparison, we present particle data taken directly from the PIC simulation in Figs. 4(f, g). This confirms the general form of the reconstructed distribution, and illustrates a key advantage of the orbit tracing method, in that the resolution we can achieve in both space and velocity space is much higher due to our ability to select as many velocity points as necessary (here we used 200^3). Vlasov codes for reconnection solve directly for f with little noise and may be a desirable tool for further exploration of the fine scale structures uncovered here.

The structure of the distribution also accounts for the momentum balance in the direction of the reconnection electric field. Close to the x-line, B vanishes and the off-diagonal terms of the pressure tensor are dominant, balancing the electric field

$$E_y \simeq -\frac{1}{ne}\left(\nabla\cdot\mathbf{P}\right)_y = -\frac{1}{ne}\left(\frac{\partial P_{xy}}{\partial x} + \frac{\partial P_{yz}}{\partial z}\right) \quad (2)$$

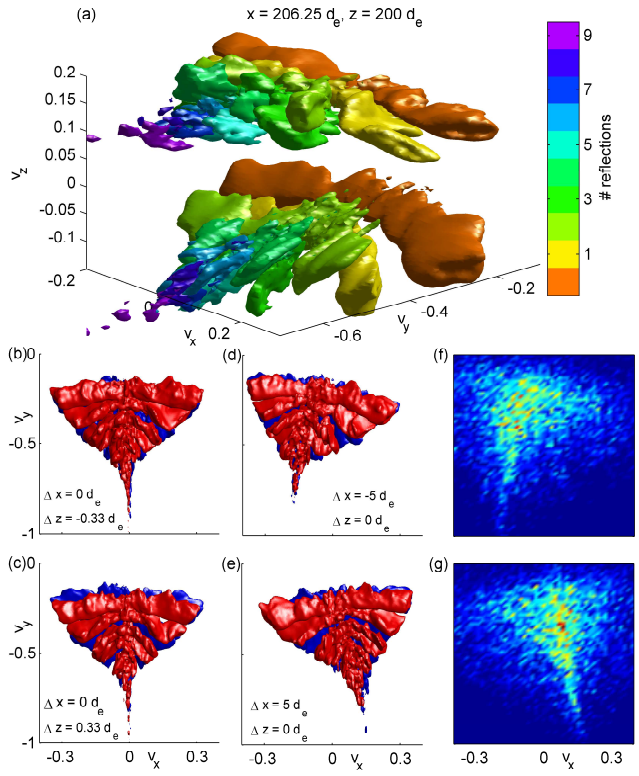

FIG. 4. Electron distribution within neutral sheet. (a) Isosurface of the distribution at x-line. The different colors correspond to the number of times the electrons are reflected in the layer. (b), (c) Isosurfaces of the distribution at $\Delta z = \pm 0.33 d_e$ above and below x-line at $(x, z) = (206.25, 200)$. The red region lies in $v_z > 0$, the blue in $v_z < 0$. Note the relative displacement in v_y of the red and blue surfaces as z increases, causing a gradient in P_{yz}. (d), (e) Isosurfaces of the distribution at $\Delta x = \pm 5 d_e$ to the left and right of the x-line. Rotation of the distribution along the layer causes the gradient in P_{xy}. (f), (g) v_x-v_y distribution of particles taken from PIC simulation at $\Delta x = \pm 5 d_e$.

where the frozen in condition $\mathbf{E} + \mathbf{v} \times \mathbf{B} = 0$ is broken by electron meandering motion [11, 12]. These terms arise from the small changes in the distribution function between different positions. In Figs. 4(b, c) (and Fig. 3(a)), moving from below to above x-line, we observe that the $v_z < 0$ portion of the distribution begins slightly displaced in the negative v_y direction relative to the $v_z > 0$ portion and ends slightly displaced in the positive v_y direction, giving rise to a gradient in P_{yz}. The gradient in the P_{xy} term arises from the rotation of the distribution in the v_x-v_y plane as one moves along x, which is shown in Figs. 4(d, e). For the present simulations we find that $\partial P_{xy}/\partial x$ is most important for balancing E_y as its magnitude depends most strongly on the force associated with E_y, whereas the magnitude of $\partial P_{yz}/\partial z$ is generic to the layer, insensitive to E_y.

To summarize, we have shown how the inflow electron pressure anisotropy is responsible for the structure of the electron diffusion region in anti-parallel reconnection, and that the current integrated across the layer is insensitive to the reconnection electric field. The incoming electrons into the layer stream along field lines with little perpendicular velocity. Their entry location determines their initial velocity in the out-of-plane y-direction and depending on the number of bounces in the layer, v_y is further increased by magnetic force turning part of the initial v_x into the y-direction. This yields highly structured and striated electron distributions uncovered here for the first time. The reconnection electric field, E_y is responsible for more subtle structures in f, important for momentum balance at the x-line.

This work was funded in part by NASA grant NNX10AL11G, an NSF CAREER grant 0844620 at MIT and by the NASA Heliophysics Theory Program at LANL.

[1] S. von Goeler, W. Stodiek, and N. Sauthoff, Phys. Rev. Lett. **33**, 1201 (1974).
[2] M. Yamada, R. Kulsrud, and H. Ji, Rev. Mod. Phys. **82**, 603 (2010).
[3] M. Oieroset, R. P. Lin, T. D. Phan, D. E. Larson, and S. D. Bale, Phys. Rev. Lett. **89**, 195001 (2002).
[4] J. Egedal, M. Oieroset, W. Fox, and R. P. Lin, Phys. Rev. Lett. **94**, 025006 (2005).
[5] L.-J. Chen, N. Bessho, B. Lefebvre, H. Vaith, A. Fazakerley, A. Bhattacharjee, P. Puhl-Quinn, A.Runov, Y. Khotyaintsev, A. Vaivads, et al., J. Geophys. Res **113**, A12213 (2008).
[6] W. Daughton, J. Scudder, and H. Karimabadi, Physics of Plasmas **13**, 072101 (pages 15) (2006),
[7] A. Le, J. Egedal, W. Daughton, J. F. Drake, W. Fox, and N. Katz, Geophys. Res. Lett. **37**, L03106 (2010).
[8] A. Le, J. Egedal, W. Daughton, W. Fox, and N. Katz, Phys. Rev. Lett. **102**, 085001 (2009).
[9] J. Egedal, W. Fox, N. Katz, M. Porkolab, M. Oieroset, R. P. Lin, W. Daughton, and J. F. Drake, J. Geophys. Res **113**, A12207 (2008).
[10] R. Horiuchi and H. Ohtani, Commun. Comput. Phys **4**, 496 (2008).
[11] A. Ishizawa, R. Horiuchi, and H. Ohtani, Physics of Plasmas **11**, 3579 (2004),
[12] M. Hesse, S. Zenitani, and A. Klimas, Physics of Plasmas, **15** (2008), ISSN 1070-664X, doi:10.1063/1.3006341